A Least Square Algorithm for Optimal Heater Placement in Microsensors

C. C. Liu, P. F. Man, and C. H. Mastrangelo
Center for Integrated Sensors and Circuits
Department of Electrical Engineering and Computer Science
University of Michigan
Rm. 2405, EECS Bldg., Ann Arbor, MI 48109-2122, USA

ABSTRACT

In this paper we present an algorithm that yields the optimal placement of a finite number of constant power density heaters for an arbitrary desired temperature profile. Using this algorithm, the volume efficiency (the percentage of volume heated within target temperature) can be optimized using different number of heaters. For an example heating chamber, the optimized heater placement method yields 76% volume efficiency using three heaters which is close to the ultimate volume efficiency of 84 %. This is a three-fold improvement over the 26% volume efficiency achievable using a single heater. The performance of the algorithm and the resulting improvements in temperature uniformity were determined experimentally using a thermal imaging microscope.

Keywords: Least square optimization, microsensor, microchamber

INTRODUCTION

Precise temperature control of heated surfaces and control volumes is of critical importance in a wide variety of thermally activated devices used for chemical analyses such as conductivity-type gas sensors, microcalorimeters [1], and chemical reaction chambers for biological assays [2][3]. Due to their Ahrrenius-type characteristics, the performance of these devices depends strongly on their temperature uniformity; hence the proper use of heaters becomes a major design consideration. Often, the use of a single heater in these devices fails to achieve the necessary uniform temperature distribution. The uniformity can be improved using several independent heaters, but the proper heater placement must be determined as incorrectly placed heaters lead to temperature profiles that are too hot or too cold at particular spots.

In this paper we present an algorithm that yields the optimal placement of a finite number of constant power density heaters for an arbitrary desired temperature profile. This method was applied to the design of a specific heating microchamber; however, it is general enough for arbitrary heated structures. The improvement on the temperature profile uniformity was experimentally verified using an infrared thermal microscope. In this paper, we first discuss the algorithm followed by a design example, multiple heater performance comparisons, experimental data verification, and a brief summary.

THEORY

Temperature distribution is often numerically determined by finite difference or finite elements. In the first step, the structure is characterized in terms of a nodal (or element) network. Next, by applying energy conservation principles at each node, the nodal network is transformed into a matrix of linear equations. The method described below works for all problems which generate a matrix. In the matrix formulation node temperatures are determined from the matrix equation

$$M\hat{T} = \hat{P}_{gen} \tag{1}$$

where M is the thermal conductance matrix, $\hat{T}$ the nodal temperature vector, and $\hat{P}_{gen}$ the power generation vector. This is the general form in which all heat problems appear when solved numerically in all dimensions.

Traditionally, heaters are placed at areas where they are conveniently reached. The most common approach found in the literature involves a single heater distributed throughout the structure. The placement of the heater essentially determines the nodes where $\hat{P}_{gen} > 0$. Arbitrarily placed and constant P_{gen} undoubtedly yields nonuniform temperature profiles.

In our approach, the placement and power of each heater is determined from the actual required power distribution for a particular temperature profile. To achieve this first the nodes where the temperature is controlled (hence heated) are specified. The number of heated nodes may be initially large, but we shall show that in most cases, only a few strategic heater locations are needed to maintain the structure at a well controlled temperature. Therefore the matrix nodes are split into nodes with heaters and nodes without heaters, and matrix M can now be subdivided into four submatrices.

$$\begin{bmatrix} M_{11} M_{12} \\ M_{21} M_{22} \end{bmatrix} \begin{bmatrix} \hat{T}_{Heaters} \\ \hat{T}_{others} \end{bmatrix} = \begin{bmatrix} \hat{P}_{gen} \\ 0 \end{bmatrix} \tag{2}$$

or

$$
\begin{aligned}
M_{11}\hat{T}_{Heaters} + M_{12}\hat{T}_{others} &= \hat{P}_{gen} \\
M_{21}\hat{T}_{Heaters} + M_{22}\hat{T}_{others} &= 0
\end{aligned} \quad (3)
$$

Solving equation 3 yields

$$\hat{T}_{others} = -M_{22}^{-1}M_{21}\hat{T}_{Heaters} \quad (4)$$

Back-substitution of this result into the matrix equation yields the required heater power distribution

$$\hat{P}_{gen} = (M_{11} - M_{12}M_{22}^{-1}M_{21})\hat{T}_{Heaters} \quad (5)$$

Therefore when $\hat{T}_{Heaters}$ is specified $\hat{P}_{gen}$ is uniquely determined.

For complicated geometries, the construction and manipulation of the conductance matrix and the calculation of heat fluxes is performed using a finite element program. First, the desired temperature boundary conditions are applied to the microstructure at the heated surface, and the temperature is solved everywhere using a conventional FEM solver (such as ANSYS). Next, the integrated total heat flux over each node of the heated surface, Q_i, is calculated using an external surface integral. This represents the heat required to leave each of

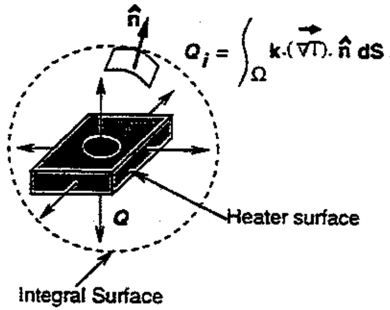

Figure 1: Surface integral of heater node

the heaters nodes necessary to yield the desired temperature profile at the heater surface.

The specification of temperature over other surfaces can also result in non-heater elements with net power generation. Under this method, these power is unaccounted; therefore precise temperature control can only be achieved near the heated surfaces. This difficulty can be overcome using good insulating materials for unheated surfaces.

The element heat density is next calculated

$$\rho_i = Q_i/dV_i \quad (6)$$

where dV_i is the element volume associated with the node. For N nodes, an exact profile could be achieved at the heater surface with N heaters of heat density Q_i. In practice, this power density must be approximated with a finite number of constant power density heaters (ie. resistive wires).

In order to achieve this we first sort out the discrete Q_i in decreasing order thus forming a coordinate independent power density histogram $\tilde{f}$ and a corresponding node map $\mathcal{M}(i)$ as shown in Fig. 2.

$$Q_i(x_i, y_i) \overset{sort}{\rightarrow} \tilde{f}(\mathcal{M}(i)) \quad (7)$$

The resulting histogram is a monotonically decreasing function of the now mapped node number. A smooth

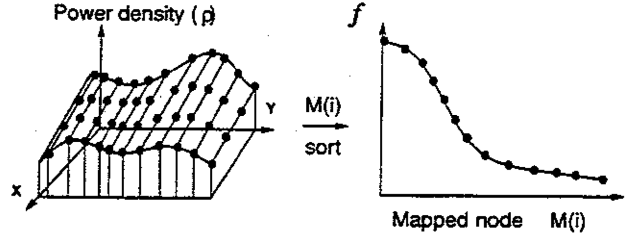

Figure 2: Construction of one dimensional mapped power density histogram

power distribution f is then constructed using an interpolating spline. This density is next approximated with step functions of uniform power. The width W of the steps specifies the extent of the heating wire while its height a specifies its uniform power. In the procedure, the continuous representation instead of the discrete one is used because it yields the use of continuous optimization techniques. The continuous representation permits heater sizes of fractional length which are later snapped to the underlying discrete mesh.

The power density is now a function of coordinate x which represents the sorted mapped node number. For a one heater approximation, the square error function ε_1^2 is constructed

$$\varepsilon_1^2 = \int_0^{W_1} (f(x) - a_1)^2 dx + \int_{W_1}^{\infty} f(x)^2 dx \quad (8)$$

The error is minimized when

$$f(W_1) = \frac{a_1}{2} \quad (9)$$

$$a_1 = \frac{1}{W_1}\int_0^{W_1} f(x)dx \quad (10)$$

The generalized expression for the error function ε_n^2 for n heaters is

$$\varepsilon_n^2 = \sum_{i=1}^{n}\int_{W_i}(f(x) - a_i)^2 dx + \int_{\sum_{i=1}^{n} W_i}^{\infty} f(x)^2 dx \quad (11)$$

which is minimized when

$$a_i = \frac{1}{W_i}\int_{W_i} f(x)dx \quad (12)$$

$$f(\sum_{i=1}^{k} W_i) = \frac{a_k + a_{k+1}}{2} \quad (13)$$

$$f(\sum_{i=1}^{n} W_i) = \frac{a_n}{2} \quad (14)$$

These expressions may be satisfied for several configurations; therefore a global minimizer must be used. In this paper we use the downhill simplex minimization method [4]. Figures 3 and 4 show an example of the heat flux approximation using one and three heaters. By repeating

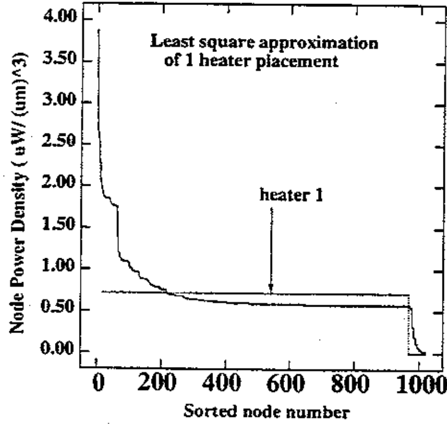

Figure 3: Sorted node power density distribution and one heater approximation

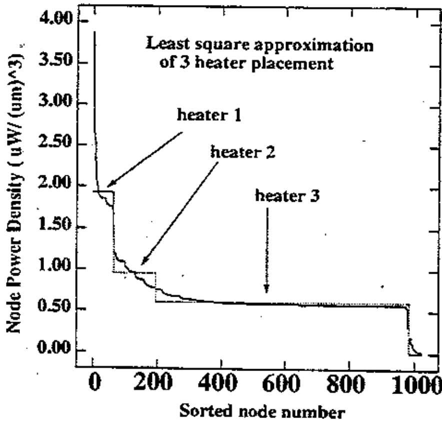

Figure 4: Three heater approximation

this algorithm, the minimization of square error can be achieved using an arbitrary number of heaters. The selection of the number of heaters results in a compromise between the complexity of heater placement routing and the desired efficiency.

After the discrete heater locations are determined, the required amount of power generated in the heater is specified and the desired temperature profile boundary conditions are removed. The temperature of the structure is next re-calculated with the FEM solver and compared to the desired values to determine the method of effectiveness.

The procedure is summarized in the flowchart shown below.

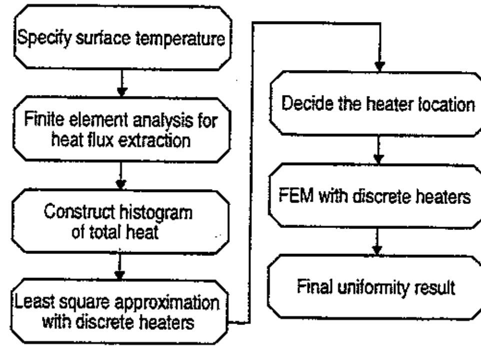

Figure 5: Flow chart of heater placement algorithm

EXAMPLE

The heater generation method was applied to a microfabricated DNA amplification chamber shown in the schematic of Fig. 6. The test chamber consists of a

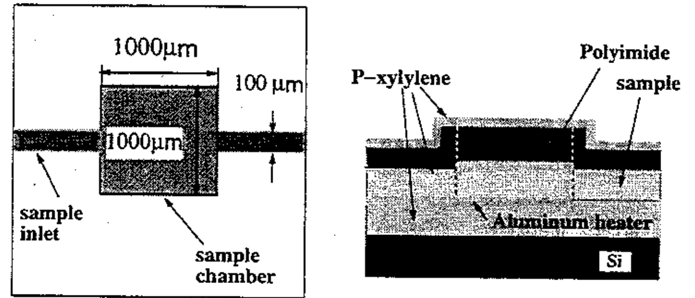

Figure 6: Schematic of the test chamber

50 μm p-xylylene layer deposited on top of a silicon wafer. A 5000 Å Aluminum (Al) heater layer is next deposited on top of the insulating plastic. The Al heater is covered by a second 2 μm p-xylylene layer followed by 20 μm of the sample. The chamber ceiling is formed by a composite sandwich layer of 2 μm p-xylylene, 20 μm polyimide and the last 2 μm p-xylylene. Figure 7 shows the optimal three heater arrangement (with f shown in Fig. 4) and the discretization of the power distribution in one quarter of the chamber. The target temperature in this design is aimed at 94 °C. The

Table 1: Heater power dissipation

heater location	Power density	Power dissipation
Base heater	0.6 $\mu W/\mu m^3$	103.57 mW
Middle heater	0.96 $\mu W/\mu m^3$	20.06 mW
Edge heater	1.93 $\mu W/\mu m^3$	21.16 mW

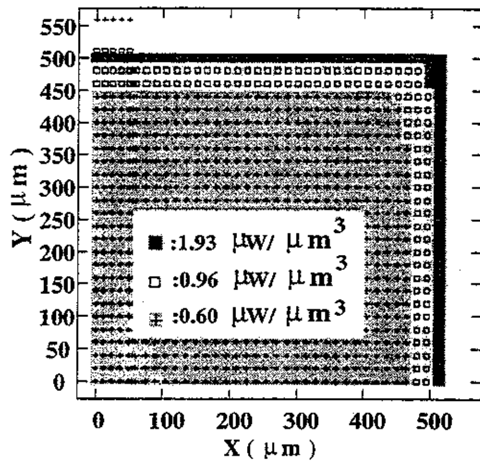

Figure 7: Optimal three heater arrangement

two heaters with the largest power density are located at the periphery of the chamber. These heaters account for the power leaving the chamber parallel to the substrate. The third heater occupies most of the central region and compensates for power losses to the underline substrate normal to the surface. Using these discrete heaters the temperature inside the chamber was re-calculated in the absence of the temperature forcing boundary condition. Figure 8 shows the volume efficiency of the one, two, and three heater approximations at 94 °C (26%, 43% and 74%, correspondingly). The algorithm yields tem-

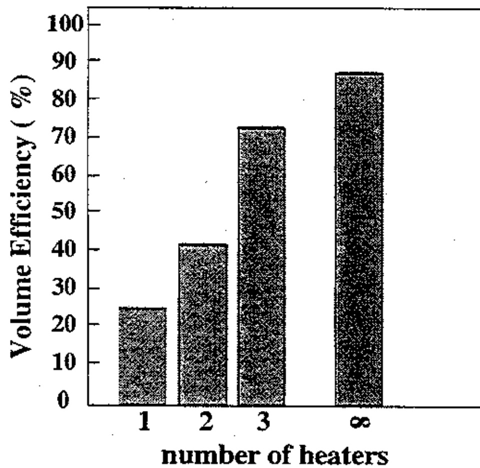

Figure 8: Three heater placement performance

perature uniformities within the required ±1.5 °C window inside 74.1 % of its volume using only three heaters. The three heater configuration has an efficiency roughly three times larger than that for the single heater design. Figures 9 and 10 show three dimensional plots of temperature within the chamber indicating the improved uniformity.

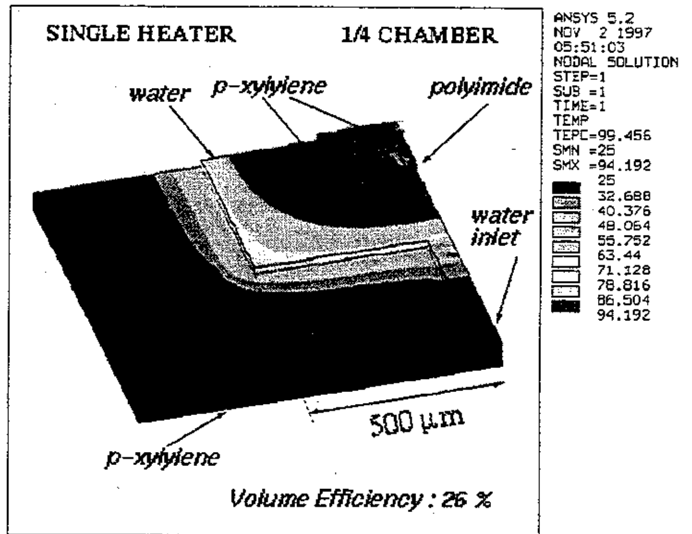

Figure 9: Temperature contours with one heater element

EXPERIMENTS

In order to determine the effectiveness of the method, a 20 μm-high all p-xylylene chamber was constructed on a silicon substrate using the plastic micromachining process developed by Man [5], [6]. Because of the limitation of the thickness of p-xylylene on top of silicon, the bottom isolation p-xylylene was 10 μm and the top walls are 10 μm thick. The heaters for the chamber were designed according to the method outlined above. The SEM of fabricated device is shown in Fig. 11 and the optical photograph is shown in Fig. 12. The chamber has nine pillars that support the structure and prevent the top wall from collapsing. The base heater consists of a serpentine Ti/Al heater. Ideally, it dissipates the same amount of heat flux under the assumption that the wire resistance is uniformly distributed across the entire base plane. After devices were fabricated, they were mounted on dual-in-line ceramic packages and wire bonded.

In this experimental verification, we measured the temperature uniformity of the top chamber wall when one and two heaters are powered up. A target temperature of 45 °C was used to minimize the water vaporization rate during the temperature measurements. De-ionized water is injected into the chamber using a micropipette, and the heaters were next powered up under an infrared thermal microscope (Computherm, Barnes Engineering) at NIST (National Institute of Standard Technology), Gaithersburg, MD. Figures 13 and 14 show measured radiance ($\epsilon_o \sigma T^4$) for the device with one and two heaters powered up.

From the radiance data, the temperature uniformities were calculated. For the one heater system, Fig. 13 indicates that 42.5 % of interior volume is within ±1.0 °C under the 2-D topview from the thermal micro-

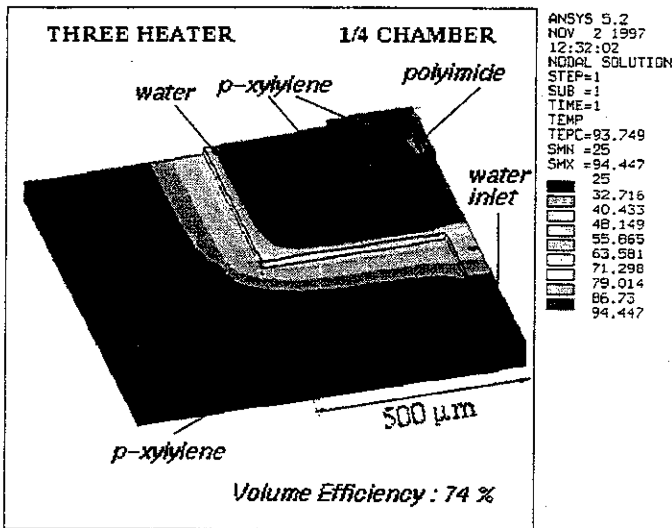

Figure 10: Temperature contours with three heater elements

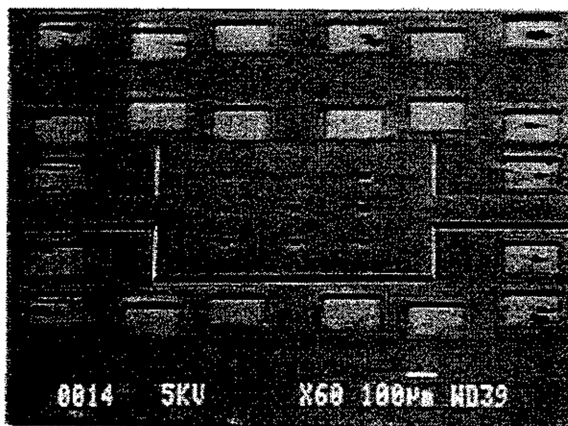

Figure 11: SEM of microchamber

scope. Simulated results predict that 43.6 % of the internal volume meets the temperature specification. The total power consumption of this base heater is 184.91 mW. Therefore, the simulation is very close to testing data. Figure 14 shows the measured radiance of a chamber with two powered heaters. Using almost the same amount of power (185.51 mW), the testing data shows an improvement in the temperature uniformity indicating that 50.56 % of the internal volume is with specifications. The simulated value was 53.2 % in good agreement with the radiance data.

LIMITATIONS AND IMPROVEMENTS

The method described above is effective in improving the temperature uniformity of heated microdevices, but it has several limitations. First and foremost, good temperature control can only be achieved in the regions near the heated surfaces; therefore high insulation walls are required. In addition, the mapping method makes the assumption that nodal heaters placed along the heated surface can be interconnected arbitrarily. The routing may not be achievable if a complex heater pattern is found. Also in some situations, the heater power may be negative and hence unrealizable.

In addition, the calculation must account for the conduction of the heaters *a-priori* before they are actually found. In other words, the conduction of heat through the heater layers must be estimated before the heaters are defined. Under the cases discussed, the heaters covered most of the base plate; therefore the conduction was simply accounted by assuming that a layer of aluminum was uniformly embedded within the heated surface (out of which the heaters are separated and constructed).

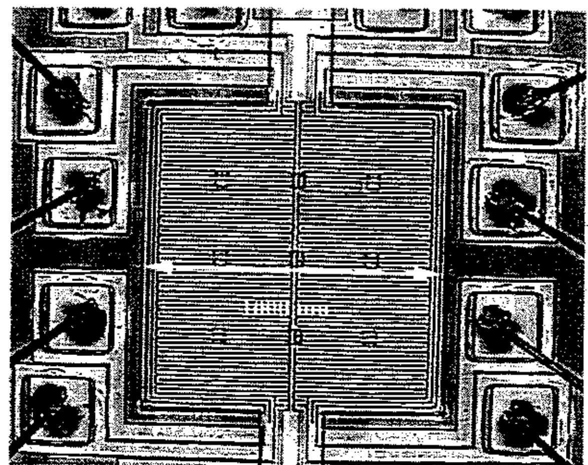

Figure 12: Optical photograph of fabricated p-xylylene microchamber

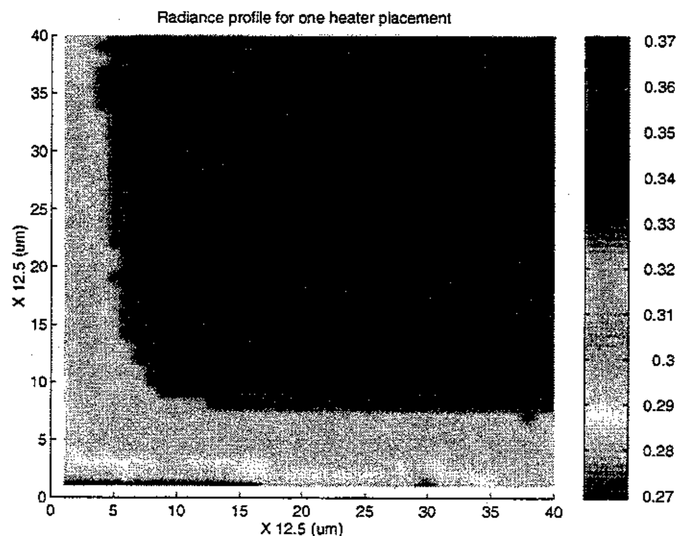

Figure 13: Measured radiance with one heater turned on

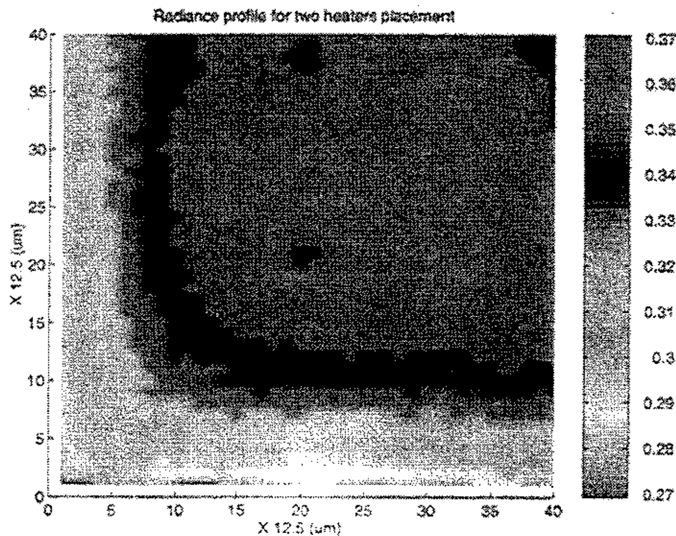

Figure 14: Measured radiance with two heaters turned on

In other situations where the heater locations are more sparse, the influence of the heater must be accounted for in an iterative manner, since the heater definition alters the conductance matrix M.

The current method approximates the actual heat flux distribution at the heated surface. This gives an optimal representation of the heat flux but not necessarily the resulting temperature. Alternatively, the optimization could be aimed to maximize the temperature uniformity and volume efficiency directly.

SUMMARY

In this paper we present an algorithm which yields optimal heater configurations for arbitrary temperature profiles. The method solves heat fluxes first using conventional FEM tools and next constructs a power histogram that is approximated with step functions representing each heater. The method was tested with several examples and indicated a three-fold improvement in the volume heating efficiency of microfabricated chambers. An experimental verification using infrared microscope is also demonstrated.

ACKNOWLEDGEMENTS

The authors wish to thank Dr. David Blackburn, Dr. John Suehle, Dr. Allen Hefner Jr., and Dr. Michael Gaitan in NIST for their kind help with the NIST infrared imager microscope. This project was partially supported by the National Institute of Health and the Semiconductor Research Corporation.

REFERENCES

[1] M. Zanini, J. H. Visser, L. Rimai, R. E. Soltis, A. Kovalchuk, D. W. Hoffman, E. M. Logothetis, U. Bonne, L. Brewer, O. W. Bynum, and M. A. Richard, "Fabrication and properties of a Si-based high-sensitivity microcalorimetric gas sensor," *Sensors and Actuators*, vol. A48, pp. 187–192, 1995.

[2] M. A. Northrup, M. T. Ching, R. M. White, and R. T. Watson, "DNA amplification with a microfabricated reaction chamber," in *Proc. 1993 IEEE Int. Conf. Solid-State Sens. Actuat.*, pp. 924–926, 1993.

[3] Y. T. Hsueh, R. L. Smith, and M. A. Northrup, "A microfabricated electrochemiluminescence cell for the detection of amplified DNA," in *Transducer's 95*, pp. 768–771, 1995.

[4] The MathWorks, Inc., *MATLAB Reference Guide*. Natick,MA: The MathWorks Inc., 1992.

[5] P. F. Man, D. K. Jones, and C. H. Mastrangelo, "Microfluidic plastic capillaries on silicon substrates: a new inexpensive technology for bioanalysis chips," in *International Workshop on Micro Electromechanical Systems (MEMS 97)*, pp. 311–316, 1997.

[6] P. F. Man, C. H. Mastrangelo, M. A. Burns, and D. T. Burke, "Microfabricated capillarity-driven stop valve and sample injector," in *International Conference on Micro Electromechanical Systems (MEMS 98)*, pp. 45–50, 1997.